

## Article

# The Rheological Properties and Strength Characteristics of Cemented Paste Backfill with Air-Entraining Agent

Baogui Yang<sup>1</sup>, Xiaolong Wang<sup>1,\*</sup>, Peng Yin<sup>2</sup>, Chengjin Gu<sup>1</sup>, Xindong Yin<sup>3</sup>, Faguang Yang<sup>1</sup> and Tao Li<sup>1</sup><sup>1</sup> School of Energy and Mining Engineering, China University of Mining and Technology, Beijing 100083, China<sup>2</sup> COSCO Shipping (Qingdao) Co., Ltd., Qingdao 266000, China<sup>3</sup> Chifeng Chaihulanzi Gold Mining Co., Ltd., Chifeng 024039, China

\* Correspondence: bq1900101030@student.cumtb.edu.cn; Tel.: +86-13161020229

**Abstract:** Clogging pipelines is one of the most common and urgent problems in paste backfill mining. The aim of the present study was to solve the problem of pipe blockage in paste backfill mining. In this paper, paste mixed with coal gangue, fly ash, cement, and additives is used to investigate the influence of three air-entraining agents (AEAs) (including sodium dodecyl sulfate (SDS), triterpene saponin (SJ), and sodium abietate (SA)) on the flow characteristics and strength characteristics of the paste. A series of relevant tests was conducted on the paste, such as air content experiments, slump and expansion experiments, viscosity and yield stress tests, and the uniaxial compressive strength (UCS) test. The results show that the air content of the paste increases with increasing AEA content, but the increase is limited and reaches a maximum at 0.9 AEA. The slump of the paste increased by up to 10–13 mm, and expansion increased by up to 66–130 mm compared to the paste without AEA. The viscosity of the paste decreased by up to 0.13–0.20 Pa·s, and the yield stress decreased by 81.47%–93.7% of the original. The strength of the paste was also reduced, and after 28 days of curing, the strength was reduced by up to 1–1.2 MPa. Taking into account the strength requirement of 3 MPa for the paste from the Linxi mine, it was considered that the dosage of 0.9 B was a good choice, as it could better change the flowability of the paste and reduce the pipeline transportation resistance and transportation energy consumption. At the same time, the strength was also acceptable. The study in this paper can provide a reference for performance studies of pastes mixed with coal gangue, fly ash, cement, and additives as materials.

**Keywords:** air-entraining agent; paste backfill; air content; rheological properties; strength characteristics

**Citation:** Yang, B.; Wang, X.; Yin, P.; Gu, C.; Yin, X.; Yang, F.; Li, T. The Rheological Properties and Strength Characteristics of Cemented Paste Backfill with Air-Entraining Agent. *Minerals* **2022**, *12*, 1457. <https://doi.org/10.3390/min12111457>

Academic Editors: Gianvito Scaringi, Haigiang Jiang, Liang Cui, Nan Zhou and Xiwei Zhang

Received: 26 October 2022

Accepted: 17 November 2022

Published: 18 November 2022

**Publisher's Note:** MDPI stays neutral with regard to jurisdictional claims in published maps and institutional affiliations.



**Copyright:** © 2022 by the authors. Licensee MDPI, Basel, Switzerland. This article is an open access article distributed under the terms and conditions of the Creative Commons Attribution (CC BY) license (<https://creativecommons.org/licenses/by/4.0/>).

## 1. Introduction

Coal is one of the main energy sources around the world, especially in China. It can be seen from Figure 1 that coal provided more than 60% of China's primary energy from 2012 to 2021. It is an important energy source in China [1]. That is why coal mining activities have been so frequent in China.

As one of the most important sources of power in industry, coal plays an important role in the social and economic development of human beings in most countries around the world [2]. With the progress of human civilization, there have been worldwide demands on coal to improve living standards; therefore, more and more coal is being mined [3]. When mining activities are frequent, the environmental pollution and casualties caused by mining activities become more and more serious [4,5]. Coal gangue occupies 15%–20% of the mined minerals from coal mines [6]. If left untreated and left to pile up on the surface, it will occupy a large amount of land. Coal gangue storage represents about 6 billion tons, and the land occupied by gangue is about 133 sq. km. This amount increases at the rate of 500 million to 800 million t/a [7–9]. At the same time, the resulting dust will pollute the air, and the leached harmful substances will pollute the surface water [10,11]. Paste backfill is recognized as a method to solve this problem [12,13].

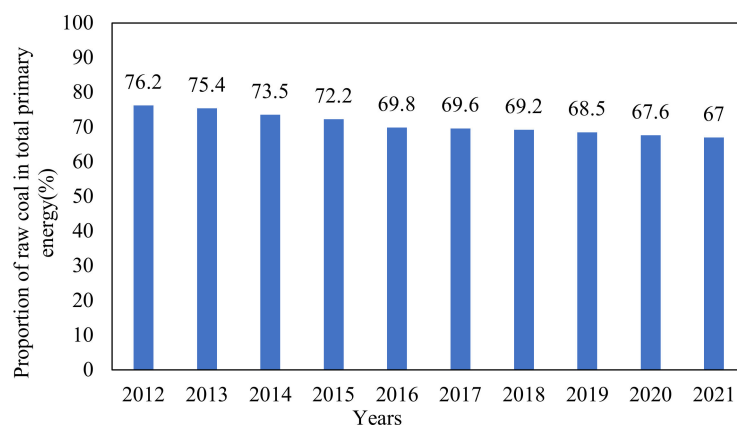


**Figure 1.** The proportion of raw coal in total primary energy from 2012 to 2021 in China (data from the National Bureau of Statistics China).

Paste backfill mining was first used in metal mining. Due to its superiority in handling the solid waste from mines, it has gradually been introduced into coal mines in recent years [14–21]. Coal mine paste backfilling uses coal gangue, a solid waste from coal mines, and fly ash, a waste from thermal power plants, as the main materials and cement as the binder. These materials are mixed with water to form a paste [22,23]. Some high-quality coal is stored under towns and cities, such as the Linxi mine in China. Using paste backfill can not only reduce the damage incurred by coal gangue to the environment, but can also fill the space in which coal has been mined, so that the ground surface does not cave in and to ensure that the ground buildings are not destroyed [3,24]. Therefore, more and more coal mines are trying to use paste backfilling. One of the most common and urgent problems faced when implementing paste backfill mining is clogging in the pipelines [25,26].

Due to the larger area of coal deposits, paste needs to be transported over long distances (2500 to 3000 m) during backfilling. Long-distance transportation puts higher demands on the pumpability of the paste [27,28]. At the same time, the particle size of gangue is larger (max 10 mm after crushing) and much larger than the particle size of the tailings (max 1 mm) [3]. Thus, the liquidity performance of mixed paste in the process of transporting it is poor, making it easy to block pipes. Such blockages will cause the project progress to stop, and it also takes time and money to clean the pipes [29]. The problem of pipe plugging has plagued coal miners for a long time. Improving the fluidity of the paste can effectively solve the problem [30].

To solve the problem of pipe blockage caused by the settling of paste, researchers have added suspension agents to paste [31]. A suspension agent can make the gangue in the paste be suspended in the process of transportation and reduce its friction with the pipe. This guarantees the homogeneity and suspension of the paste [32]. However, the addition of a suspension agent will increase the viscosity of the paste, worsening the fluidity of the paste [33,34]. This paper selects a suitable AEA to improve the fluidity of the filling paste.

Current research on AEAs has focused on enhancing the flow properties of concrete [35,36]. Puthipad, N. et al., investigated the role of AEAs in self-compacting concrete containing water-reducing agents and found that the addition of AEA to the mixture after a highly efficient water-reducing agent (SP) inhibited the agglomeration of air bubbles [37]. Guoju Ke et al., compared the effects of six concrete AEAs in different media. The results showed that AEAs with better air-entraining properties resulted in higher initial cement paste foam heights and lower mortar densities [38]. Cao, Liang et al., determined the rheological properties and consistency of cement mortar (CM) containing AEAs at different curing times. The AEAs were found to improve the rheological properties of the paste [39].

Several people have studied the mechanism of the effect of AEAs on the strength of paste. Youzhi Zhang et al., investigated the effect of sodium dodecyl sulfate (SDS), an AEA, on the uniaxial compressive strength (UCS) of cemented paste backfill (CPB). The results showed that the UCS of CPB increased and then decreased as the initial air content in the

fresh slurry increased. The addition of AEA has a certain delay-hindering effect on the cement hydration reaction. It was also demonstrated that it decreases the UCS of CPB [40]. The effect of air entrainment on the UCS of foam mine fill (FMF) was investigated by Hefni, M et al., The UCS of FMF samples was 20%–50% lower relative to the reference sample without entrained air [36,41,42].

It is worth mentioning that these studies used tailings rather than gangue. Additionally, there are no studies on the effects of AEA on paste made from coal gangue. Therefore, in this paper, the effect of AEAs on the flow characteristics and strength characteristics of the paste was investigated when mixed with gangue.

## 2. Experiment

### 2.1. Materials

#### 2.1.1. Gangue

Coal gangue is the most important solid waste produced in the process of coal mining and washing. Since gangue is symbiotic with coal, gangue also contains carbon and mainly contains two elements: silicon and aluminum. It is generally the product of oxidation and some trace elements such as sulfur, iron, calcium, etc. [24]. The gangue from the Linxi mine was analyzed with an energy spectrum semi-quantitative analyzer. The results are shown in Table 1. The SiO<sub>2</sub> content in the gangue is 41.86%, and the contents of CaO and Al<sub>2</sub>O<sub>3</sub> were about 23%. The gangue also contained a small amount of Fe<sub>2</sub>O<sub>3</sub>. The gangue of the Linxi mine is similar to clay rock.

**Table 1.** Chemical composition of coal gangue.

| Chemical Composition | Al <sub>2</sub> O <sub>3</sub> | SiO <sub>2</sub> | K <sub>2</sub> O | CaO   | TiO <sub>2</sub> | Fe <sub>2</sub> O <sub>3</sub> | Total |
|----------------------|--------------------------------|------------------|------------------|-------|------------------|--------------------------------|-------|
| Content (%)          | 23.43                          | 41.86            | 0.82             | 23.74 | 1.36             | 5.09                           | 100   |

#### 2.1.2. Cement

Cement acts as a binder in the slurry. In this study, 425# ordinary silicate cement was used in the paste, and the chemical composition is listed in Table 2.

**Table 2.** Chemical composition of cement.

| Density (kg · m <sup>-3</sup> ) | Chemical Composition (%) |                  |                                |                                |      |        |
|---------------------------------|--------------------------|------------------|--------------------------------|--------------------------------|------|--------|
|                                 | CaO                      | SiO <sub>2</sub> | Al <sub>2</sub> O <sub>3</sub> | Fe <sub>2</sub> O <sub>3</sub> | MgO  | Others |
| 3120                            | 65.08                    | 22.36            | 5.53                           | 3.46                           | 1.27 | 2.30   |

#### 2.1.3. Fly Ash

The particle size, chemical composition, and mineralogical composition of fly ash were measured to understand the nature of the fly ash from the Linxi power plant. The density of the compacted fly ash from the Linxi power plant was 1450 kg/m<sup>3</sup>. An OMIK LS-C (IIA) laser particle size analyzer was used to measure the particle size distribution, as shown in Figure 2. A scanning electron microscope using HITACHIS-3500N was used to perform an energy spectrum analysis of the fly ash. As shown in Table 3, two components, SiO<sub>2</sub> and Al<sub>2</sub>O<sub>3</sub>, accounted for more than 80% of the fly ash, and small amounts of K<sub>2</sub>O, CaO, TiO<sub>2</sub>, and Fe<sub>2</sub>O<sub>3</sub> coexisted in the fly ash.

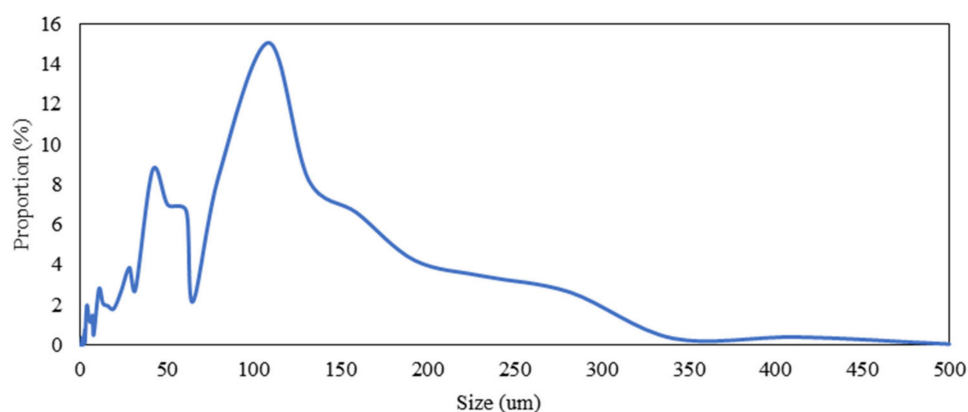


Figure 2. Particle size distribution of fly ash.

Table 3. Chemical composition of fly ash.

| Chemical Composition | Al <sub>2</sub> O <sub>3</sub> | SiO <sub>2</sub> | K <sub>2</sub> O | CaO  | TiO <sub>2</sub> | Fe <sub>2</sub> O <sub>3</sub> | Total |
|----------------------|--------------------------------|------------------|------------------|------|------------------|--------------------------------|-------|
| Content (%)          | 31.89                          | 56.89            | 1.39             | 1.84 | 1.95             | 5.38                           | 100   |

#### 2.1.4. Air-Entraining Agents

Referring to the AEAs used in the concrete industry, three types of AEA were selected for study: A—sodium dodecyl sulfate (SDS), B—triterpene saponin (SJ), and C—sodium abietate (SA). Pictures of the AEAs are shown in Figure 3.

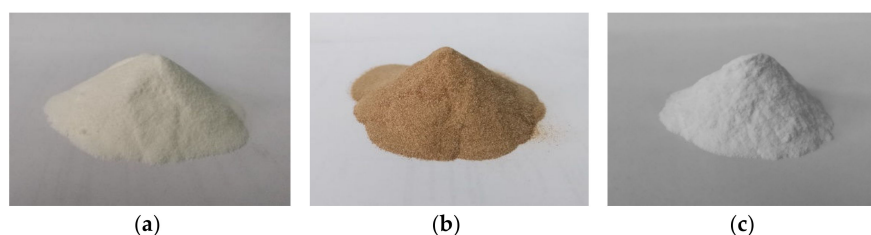


Figure 3. Pictures of AEA. (a): sodium dodecyl sulfate; (b): triterpene saponins; (c): sodium abietate.

A has good foaming ability. It can foam quickly and richly, but it degrades quickly over time. It is a white powder that is soluble in water and alcohol [43].

B belongs to the family of saponin organic compounds, which can reduce the surface tension of liquids. It is stable and easily soluble in water. When mixed with liquid, a large number of bubbles are produced in the slurry. The bubbles are small, stable, and independent [44].

C has a benzene ring structure and amphiphilic structure (hydrophilic group and oleophilic group), which can form a large number of bubbles. Generally, it is a white powder [45]. To allow the admixtures to be better mixed in the slurry, the admixtures were configured as a solution with a mass concentration of 1% [46]. Equation (1) was used to calculate the concentrations of the AEAs.

$$\text{AEA concentration (\%)} = \frac{M_A}{M_A + M_W} \quad (1)$$

where  $M_A$  is the mass of the AEAs, and  $M_W$  is the mass of water.

## 2.2. Experimental Methods

### 2.2.1. Experimental Design

The aim of the present experiments was to study the effects of AEAs on the flow properties and strength characteristics of paste with coal gangue as the aggregate. Addi-

tionally, we selected the most effective air-entraining agent. Referring to the contents of the materials in paper [23], the paste concentration was kept at 75.2%, the cement concentration was kept at 12%, the fly ash content was kept at 20.5%, the amount of suspension H was kept at 0.3%, and the ratio of various materials was kept unchanged. The contents of the AEAs were 0.0%, 0.3%, 0.6%, 0.9%, and 1.2%. The contents of the materials were calculated as in Equations (2)–(8).

$$\text{Cement dosage (\%)} = (M_{\text{cement}}/M_{\text{solids}}) \times 100 \quad (2)$$

$$\text{Fly ash dosage (\%)} = (M_{\text{fly ash}}/M_{\text{solids}}) \times 100 \quad (3)$$

$$\text{Gangue dosage (\%)} = (M_{\text{gangue}}/M_{\text{solids}}) \times 100 \quad (4)$$

$$\text{Pulp density (\%)} = [M_{\text{solids}}/(M_{\text{solids}} + M_{\text{water}})] \times 100 \quad (5)$$

$$\text{H dosage (\%)} = [M_{\text{H}}/(M_{\text{solids}} + M_{\text{water}})] \times 100 \quad (6)$$

$$\text{AEA dosage (\%)} = [M_{\text{AEA}}/(M_{\text{solids}} + M_{\text{water}})] \times 100 \quad (7)$$

$$M_{\text{solids}} = M_{\text{cement}} + M_{\text{fly ash}} + M_{\text{gangue}} + M_{\text{H}} + M_{\text{AEA}} \quad (8)$$

where  $M_{\text{cement}}$ ,  $M_{\text{fly ash}}$ ,  $M_{\text{gangue}}$ ,  $M_{\text{water}}$ ,  $M_{\text{H}}$ ,  $M_{\text{AEA}}$ , and  $M_{\text{solids}}$  are the mass of cement, fly ash, gangue, water, suspending agent H, AEAs, and solids, respectively (kg).

### 2.2.2. Slurry Mixing

The maximum particle size of coal gangue used for coal mine paste filling is generally 10–15 mm [24]. To make the particle size meet this requirement, a hammer crusher (CP-200) was utilized for crushing. Considering the chemical nature of the gangue from the Linxi mine, the maximum particle size of the gangue was set to 10 mm. The slurry was mixed with a mortar mixer (NJ-160). The mixing of the paste was divided into the following steps:

- Weighing of the raw materials according to the design table,
- Pouring the solid material into the mixing vessel and mixing it at 75 r/min for 2 min,
- Pouring water into the mixing vessel and mixing it at 75 r/min for 5 min,
- Pouring the AEA solution into the slurry and mixing it at 58 r/min for 2 min. The lower speed is to make the bubbles in the paste more stable.

A triple compression test mold (70.7 mm × 70.7 mm × 70.7 mm) was used to make the samples. To simulate the environment of the paste underground, the samples were cured by a curing box (YH-40B). The open-top samples were placed in a humidity chamber set at (25 ± 2) °C and 85% RH for curing. Figure 4 shows the experimental equipment.

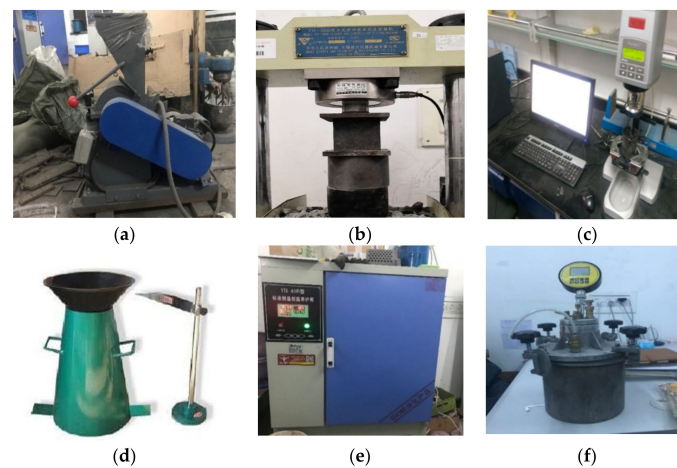


**Figure 4.** Pictures of experimental instruments and equipment (a): hammer crusher, (b): uniaxial compressive testing machine, (c): Anton Paar rheometer, (d): slump cylinder, (e): curing box, (f): digital display air content tester.

### 2.2.3. Air Content Test

The slurry was prepared according to the ratios in Table 4, and the air content was measured in the experiments according to Chinese standard JGJ/T 70-2009 [47]. The air content of the slurry was measured using a digital display air content tester (CA-3). The change in air content within 0–120 min was measured (once measured at intervals of 30 min) [48]. The specific steps of the slurry air content test are:

- After the calibration of the air content tester, fill the container with the slurry and vibrate it for 15–30 s until there are no bubbles.
- Cover the lid, tighten the clamp, and open the exhaust valve. Fill the container with water until the air outlet flows.
- Close the water injection valve and exhaust valve, open the air inlet valve, and pressurize the container to 0.1 MPa.
- Press the valve lever 1–2 times and read out the pressure value and the air content value.

**Table 4.** The proportion of experimental materials.

| Groups | Cement (%) | Fly Ash (%) | Gangue (%) | Density (%) | H (%) | AEA (%) |     |     |
|--------|------------|-------------|------------|-------------|-------|---------|-----|-----|
|        |            |             |            |             |       | A       | B   | C   |
| G-1    | 12         | 20.5        | 42.7       | 75.2        | 0.3   | 0.0     | 0.0 | 0.0 |
| G-2    | 12         | 20.5        | 42.7       | 75.2        | 0.3   | 0.3     | 0.3 | 0.3 |
| G-3    | 12         | 20.5        | 42.7       | 75.2        | 0.3   | 0.6     | 0.6 | 0.6 |
| G-4    | 12         | 20.5        | 42.7       | 75.2        | 0.3   | 0.9     | 0.9 | 0.9 |
| G-5    | 12         | 20.5        | 42.7       | 75.2        | 0.3   | 1.2     | 1.2 | 1.2 |

### 2.2.4. Slump and Expansion Test

The slump and expansion of the samples were tested according to the Chinese standard GB/T50080-2002 “Standard for Test Methods for the Performance of Ordinary Concrete Mixes”. The tests were conducted at 25 °C. Expansion measures the flow range of concrete (i.e., the diameter of the concrete flow area) [49]. The slump and expansion of the fresh slurry were measured with a slump cylinder (100 mm × 200 mm × 300 mm) [50].

### 2.2.5. Viscosity and Yield Stress Test

The viscosity and yield stress of the fresh slurry were measured using an Anton Paar rheometer (Rheolab QC). After putting the slurry into the test vessel, the computer program was started to control the rotor rotation. The program is mainly divided into two stages. The command stage in stage I, which lasts for 10 s, sets the shear rate of the rheometer rotor to 100 r s<sup>-1</sup>. After completing the mixing for stage I, the rheometer continues to run according to the program set in stage II, and the rheometer rotor agitates the slurry from 0 to 300 r s<sup>-1</sup> with a one-way linear increase. The data from phase II were collated, and the relationship between the paste’s shear rate and shear stress was fitted into a curve to obtain the viscosity and yield stress of the slurry.

### 2.2.6. UCS Test

UCS tests were conducted with a UCS testing machine (TYE-50). The samples were tested for UCS according to the Chinese standard JGJ/T 70-2009. Prior to a UCS test, the sizes of a sample are rectified to obtain valid press surfaces. UCS tests were performed using a computer-controlled mechanical press with a load capacity of 50 KN.

## 3. Results and Analysis

### 3.1. Air Content

The results of the air content tests are presented in Table 5. Figure 5d–f shows that, for the fresh slurry, the air content in the slurry gradually increased with an increase in AEA. Taking (G-1), an AEA content of 0, as the control group, the highest air content of A is 190%, 319% for B, and 144% for C. This may be because the AEA increases the number of

tiny air bubbles in the slurry, affecting the performance of the AEA by introducing tiny air bubbles. However, the increase in air content has a limit. Compared to the air content at an AEA content of 0.9‰, when the AEA content is 1.2‰, the air content of A is 85% of the highest value; that of B is 94%, and that of C is 96%. This may be because the number of air bubbles that can be accommodated reaches the upper limit. Too many tiny air bubbles combine to form large air bubbles, and the atmospheric package is more unstable, making it harder to break [51].

Table 5. Air content of the slurry for 0–120 min.

| Groups | AEA | Dosage (‰) | Air Content (%) |        |        |        |         |
|--------|-----|------------|-----------------|--------|--------|--------|---------|
|        |     |            | 0 min           | 30 min | 60 min | 90 min | 120 min |
| G-1    | A   | 0.0        | 1.220           | 1.215  | 1.223  | 1.220  | 1.224   |
| G-2    |     | 0.3        | 1.680           | 1.455  | 1.363  | 1.378  | 1.326   |
| G-3    |     | 0.6        | 1.946           | 1.771  | 1.611  | 1.565  | 1.505   |
| G-4    |     | 0.9        | 2.326           | 2.185  | 1.785  | 1.845  | 1.707   |
| G-5    |     | 1.2        | 1.977           | 1.968  | 1.864  | 1.737  | 1.689   |
| G-6    | B   | 0.0        | 1.220           | 1.215  | 1.223  | 1.220  | 1.224   |
| G-7    |     | 0.3        | 1.877           | 1.512  | 1.561  | 1.434  | 1.22    |
| G-8    |     | 0.6        | 2.282           | 2.181  | 2.189  | 1.969  | 1.876   |
| G-9    |     | 0.9        | 3.87            | 3.497  | 3.296  | 3.125  | 2.865   |
| G-10   |     | 1.2        | 3.664           | 3.206  | 2.987  | 2.983  | 2.975   |
| G-11   | C   | 0.0        | 1.220           | 1.215  | 1.223  | 1.220  | 1.224   |
| G-12   |     | 0.3        | 1.404           | 1.275  | 1.236  | 1.210  | 1.230   |
| G-13   |     | 0.6        | 1.514           | 1.426  | 1.443  | 1.419  | 1.385   |
| G-14   |     | 0.9        | 1.768           | 1.650  | 1.581  | 1.572  | 1.570   |
| G-15   |     | 1.2        | 1.696           | 1.621  | 1.591  | 1.578  | 1.571   |

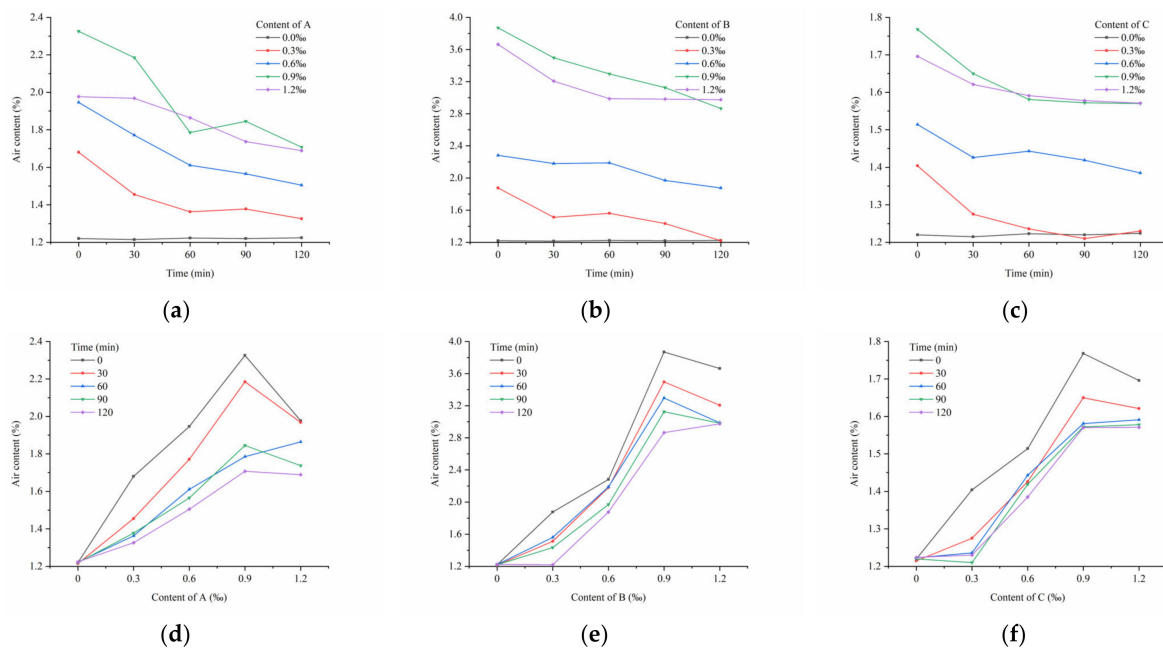


Figure 5. Air content of AEA (a): air content of A for 0–120 min, (b): air content of B for 0–120 min, (c): air content of C for 0–120 min (d): air content of A for 0–1.2‰ dosage, (e): air content of B for 0–1.2‰ dosage, (f): air content of C for 0–1.2‰ dosage.

The results for the same group of slurries are as shown in Figure 5a–c: the air content in the slurry gradually decreases with time. When the amount of AEA is 0.9‰, comparing the air content of the slurry at 0 min, the air content of A is 73.3%, 74% for B, and 88.8% for C at 120 min. The reason for this could be that some of the tiny air bubbles mixed in the slurry floated to the top and burst [52,53]. Other small bubbles merge into large bubbles.

When the bubble wall is very thin, it will burst directly into the slurry. Thus, the air content will decrease with time [37].

### 3.2. Slump and Expansion

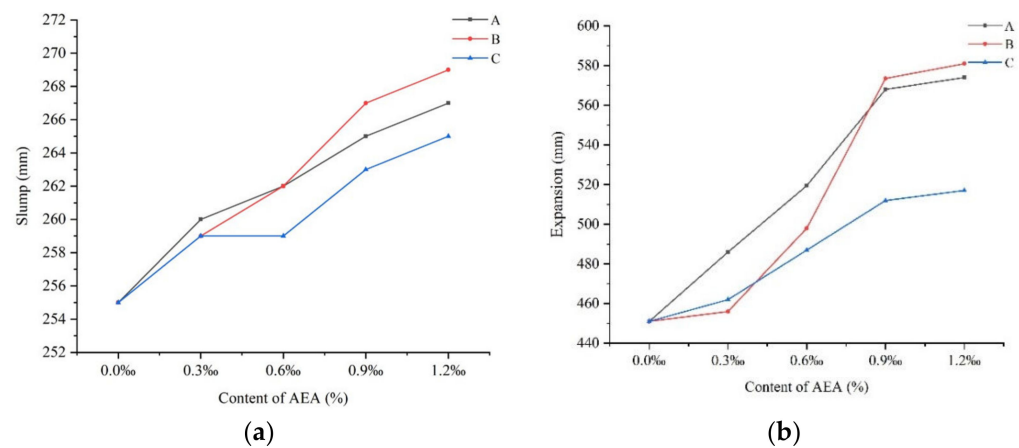
The slump and expansion are measured as shown in Figure 6. The results of the slump and expansion of the slurry are presented in Table 6. According to Figure 7a, it can be seen that the slump value of the slurry increases with an increase in AEA content. The slump of A increased by 12 mm, B increased by 14 mm, and C increased by 10 mm when the AEA content was 1.2‰ compared to 0. This shows that the slump of the slurry was improved with the addition of AEA [39,54]. This may be caused by the fact that AEA increased the number of tiny bubbles in the slurry [16,35], which resulted in the improved flowability of the slurry. With a non-changing content AEA (all at 1.2‰), the slump was 269 mm for B, 267 mm for A, and 265 mm for C. This means that B improved the slump of the slurry the most.



Figure 6. Slump and expansion tests: (a) slump, (b) expansion.

Table 6. Slump and Expansion.

| Groups | Dosage (‰) | Slump (mm)     |       |     |
|--------|------------|----------------|-------|-----|
|        |            | A              | B     | C   |
| G-1    | 0.0        | 255            | 255   | 255 |
| G-2    | 0.3        | 260            | 259   | 259 |
| G-3    | 0.6        | 262            | 262   | 259 |
| G-4    | 0.9        | 265            | 267   | 263 |
| G-5    | 1.2        | 267            | 269   | 265 |
| Groups | Dosage (‰) | Expansion (mm) |       |     |
|        |            | A              | B     | C   |
| G-1    | 0.0        | 451            | 451   | 451 |
| G-2    | 0.3        | 486            | 456   | 462 |
| G-3    | 0.6        | 519.5          | 498   | 487 |
| G-4    | 0.9        | 568            | 573.5 | 512 |
| G-5    | 1.2        | 574            | 581   | 517 |



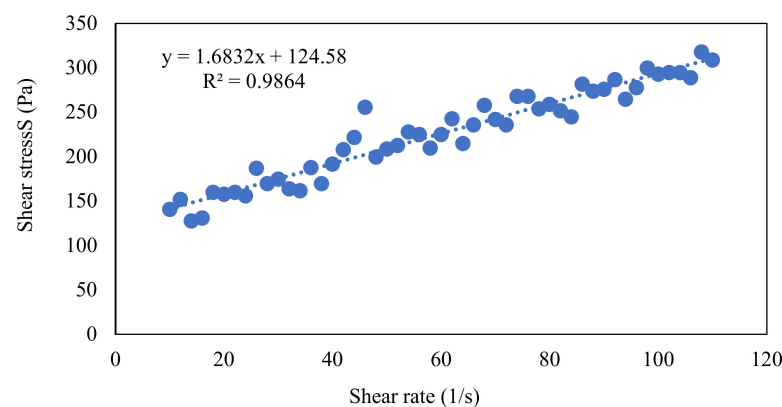
**Figure 7.** Slump and expansion of slurry with AEA. (a): Trend diagram of the slump, (b): trend diagram of the expansion.

According to Figure 7b, it can be seen that the expansion value of the slurry increases as the AEA content increases. Compared to the AEA content of 0, the expansion of A increased by 123 mm, B increased by 130 mm, and C increased by 66 mm when the AEA content was 1.2. This represents how the expansion of the slurry was improved with the addition of AEA. With the same amount of AEA (all at 1.2‰), the expansion of B was 581 mm, that of A was 574 mm, and that of C was 517 mm. This means that B improved the expansion of the slurry the most. In characterizing the flowability of the slurry, the results of the extension coincide with the slump results. The larger the test value, the better the slurry flowability.

Additionally, we can see in Figure 7a,b that, after the AEA content reached 1.2‰, the growth rate of slump and expansion became slower. This may be because too many tiny bubbles in the slurry combined into large bubbles, leading to the detachment of bubbles from the slurry. Therefore, the best value for the AEA content is 0.9‰.

### 3.3. Yield Stress and Viscosity

Tests were conducted to explore the effects of AEA on the yield stress and viscosity of the coal mine paste. The slurry was scanned for a one-way rate. Each set of tests was performed three times. The experimental results were averaged [55]. The linear regression analysis of the rheological characteristics for the paste was carried out by Excel. The functional relationship between the shear rate and the shear stress was established, as shown in the example in Figure 8. The linear regression results of the functional relationship are shown in Table 7.

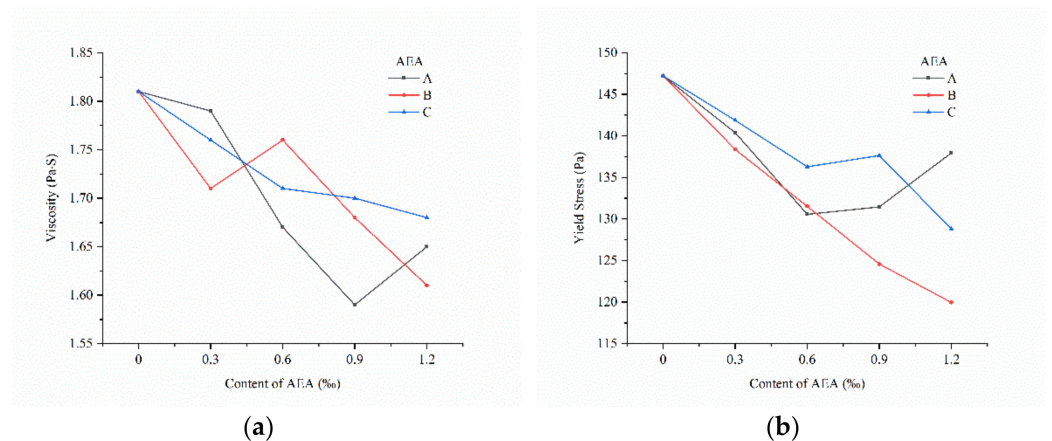


**Figure 8.** Relationship between shear stress and the shear rate of slurry B with the content of 0.9‰.

**Table 7.** Linear regression between shear rate and shear stress.

| Groups | AEA | Dosage (‰) | Regression Equation  | R <sup>2</sup> | Yield Stress (Pa) | Viscosity (Pa·s) |
|--------|-----|------------|----------------------|----------------|-------------------|------------------|
| G-1    | A   | 0.0        | $y = 1.81x + 147.23$ | 0.9327         | 147.23            | 1.81             |
| G-2    |     | 0.3        | $y = 1.79x + 140.38$ | 0.9486         | 140.38            | 1.79             |
| G-3    |     | 0.6        | $y = 1.67x + 130.57$ | 0.9883         | 130.57            | 1.67             |
| G-4    |     | 0.9        | $y = 1.59x + 131.46$ | 0.9782         | 131.46            | 1.59             |
| G-5    |     | 1.2        | $y = 1.65x + 137.95$ | 0.9892         | 137.95            | 1.65             |
| G-6    | B   | 0.0        | $y = 1.81x + 147.23$ | 0.9327         | 147.23            | 1.81             |
| G-7    |     | 0.3        | $y = 1.71x + 138.37$ | 0.9785         | 138.37            | 1.71             |
| G-8    |     | 0.6        | $y = 1.76x + 131.52$ | 0.9823         | 131.52            | 1.76             |
| G-9    |     | 0.9        | $y = 1.68x + 124.58$ | 0.9864         | 124.58            | 1.68             |
| G-10   |     | 1.2        | $y = 1.61x + 119.95$ | 0.9654         | 119.95            | 1.61             |
| G-11   | C   | 0.0        | $y = 1.81x + 147.23$ | 0.9327         | 147.23            | 1.81             |
| G-12   |     | 0.3        | $y = 1.76x + 141.88$ | 0.9625         | 141.88            | 1.76             |
| G-13   |     | 0.6        | $y = 1.71x + 136.29$ | 0.9731         | 136.29            | 1.71             |
| G-14   |     | 0.9        | $y = 1.70x + 137.63$ | 0.9283         | 137.63            | 1.70             |
| G-15   |     | 1.2        | $y = 1.68x + 128.81$ | 0.9582         | 128.81            | 1.68             |

It can be seen from Figure 9a that the viscosity of the slurry shows a decrease with the addition of AEA. When the amount of A was increased from 0 to 1.2‰, the viscosity of the slurry decreased at 0.16 Pa·s. When the amount of B was increased from 0 to 1.2‰, the viscosity of the slurry decreased at 0.2 Pa·s, and when the amount of C was increased from 0 to 1.2‰, the viscosity of the slurry decreased at 0.13 Pa·s, which means that AEA reduced the viscosity of the slurry [56]. This may be due to the large number of tiny air bubbles distributed over the whole slurry [57]. The tiny bubbles create a rolling ball effect and reduce the frictional resistance between cement, fly ash, and other substances [58]. Thus, the viscosity of the slurry is reduced.

**Figure 9.** Viscosity and yield stress of slurry with AEA: (a) viscosity of slurry with AEA; (b) yield stress of slurry with AEA.

From Figure 9b, it can be seen that the yield stress of the slurry shows a decrease with the increase in AEA. When the amount of AEA was increased to 1.2‰, the yield stress of A was 93.70% of that of the AEA content of 0, 81.47% that of B, and 87.49% that of C. The decrease in yield stress in A and C was less than that in B. This shows that B has more influence on the yield stress of the slurry.

### 3.4. Strength

The paste is transported to the target space during coal mine paste backfill [14]. The paste solidifies and hardens with the strength to achieve and support mining goals. Therefore, it is also necessary to ensure the strength of the paste [59,60]. The change in the strength of the filling body with the AEA was studied. The UCS is tested as shown in Figure 10. The results are shown in Table 8.

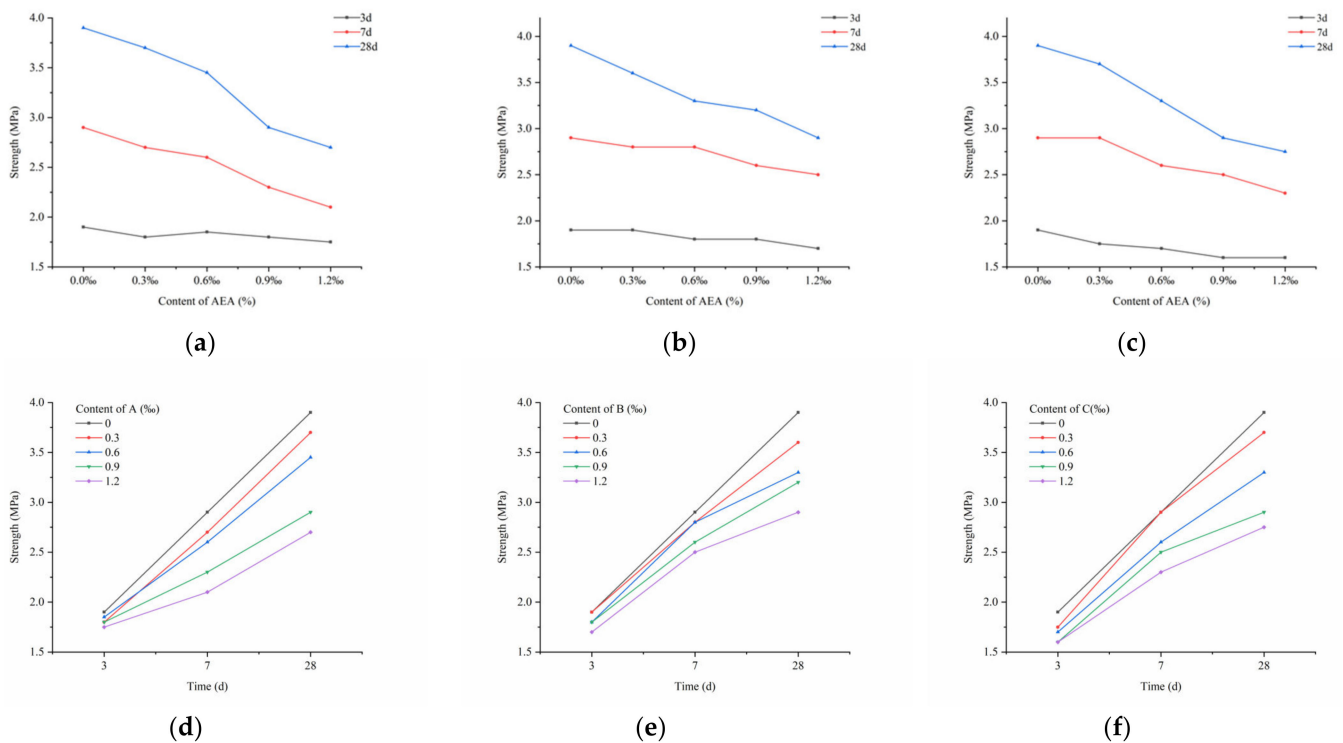


Figure 10. UCS tests: (a) sample preparation; (b) UCS test.

Table 8. Strength of paste backfilling samples.

| Groups | AEA | Dosage (‰) | Strength (MPa) |     |      |
|--------|-----|------------|----------------|-----|------|
|        |     |            | 3d             | 7d  | 28d  |
| G-1    | A   | 0.0        | 1.9            | 2.9 | 3.9  |
| G-2    |     | 0.3        | 1.8            | 2.7 | 3.7  |
| G-3    |     | 0.6        | 1.85           | 2.6 | 3.45 |
| G-4    |     | 0.9        | 1.8            | 2.3 | 2.9  |
| G-5    |     | 1.2        | 1.75           | 2.1 | 2.7  |
| G-6    | B   | 0.0        | 1.9            | 2.9 | 3.9  |
| G-7    |     | 0.3        | 1.9            | 2.8 | 3.6  |
| G-8    |     | 0.6        | 1.8            | 2.8 | 3.3  |
| G-9    |     | 0.9        | 1.8            | 2.6 | 3.2  |
| G-10   |     | 1.2        | 1.7            | 2.5 | 2.9  |
| G-11   | C   | 0.0        | 1.9            | 2.9 | 3.9  |
| G-12   |     | 0.3        | 1.75           | 2.9 | 3.7  |
| G-13   |     | 0.6        | 1.7            | 2.6 | 3.3  |
| G-14   |     | 0.9        | 1.6            | 2.5 | 2.9  |
| G-15   |     | 1.2        | 1.6            | 2.3 | 2.75 |

As shown in Figure 11a–c, in the absence of AEA, the sample strength was 1.9 MPa after 3 days of curing, 2.9 MPa after 7 days of curing, and 3.9 MPa after 28 days of curing. When the AEA content was increased from 0 to 1.2‰, the effect of AEA on strength was similar after 3 days of curing, with an approximate reduction of 0.2–0.3 MPa. After 7 days of curing, the effect of B on strength was mild, with a small reduction in strength of 0.4 MPa. C showed the second largest effect, with a reduction of 0.6 MPa. A showed the largest effect, with a reduction of 0.8 MPa. After 28 days of curing, the strength of A decreased by 0.5 MPa. After 28 days, the strength of A decreased by 1.2 MPa, the strength of B decreased by 1.0 MPa, and the strength of C decreased by 1.15 MPa. A large number of tiny air bubbles were formed in the paste via the air-entraining effect of AEA. These bubbles were distributed in the paste [61,62]. The tiny bubbles in the paste leave voids [63,64] and, therefore, the strength decreases with the addition of AEA. The larger the number of air bubbles, the larger the gaps that are formed inside [65,66].



**Figure 11.** Strength of filler with AEA: (a) strength of A dosage, (b) strength of B dosage, (c) strength of C dosage, (d) strength of the paste containing A with curing time, (e) strength of the paste containing B with curing time, and (f) strength of the paste containing C with curing time.

The variation in the uniaxial compressive strength of the paste with the curing time is shown in Figure 11d–f. It can be seen that the strength of the paste increases with the curing time. For the three AEAs, the effect of B on the strength is minimal, and the samples using B show a strength higher than 3 MPa after 28 days of curing, which meets the requirements for coal mine paste backfilling [67,68]. In conclusion, to achieve the strength requirements in the samples, using B at a dosage of 0.9‰ is the most appropriate course of action.

#### 4. Conclusions

The flow capacity of backfilling paste is crucial for filling. This paper shows the influence of AEA on slurry flow characteristics. The experiments were carried out based on the action mechanism of AEA. The following conclusions can be drawn by analyzing the test results:

- (1) AEA can form a large number of small-volume air bubbles in fresh slurry. The air content in the slurry decreases with time. With AEA content was 0 in the control group, and the highest air content of A was 109% of it, 319% for B, and 144% for C. However, the increase in air content has a limited effect. Compared to an AEA air content of 0.9‰, when the AEA content is 1.2‰, the air content of A is 85% of its highest value, 94% of that of B, and 96% of that of C. This may be because the number of air bubbles that can be accommodated reaches the upper limit, with too many tiny air bubbles combining to form large air bubbles that break easily.
- (2) AEA increases the slump and expansion of the fresh slurry. As the AEA content increases, the slump of the slurry also increased. Compared with an AEA content of 0, the slump of A increased by 12mm when the AEA content was 1.2, that of B increased by 14mm, and that of C increased by 10mm, which indicated that the slump of the slurry was improved by adding AEA. With the increase in the AEA content, the expansion of the slurry also increased. With the same AEA content (all 1.2), the expansion of B was 581 mm, that of A was 574 mm, and that of C was 517 mm. This indicates that B improved the expansion of the slurry the most. In characterizing the

flowability of the slurry, the results of the expansiveness coincide with the slump results. The larger the value tested, the better the material will flow. This is probably because AEA increases the number of tiny bubbles in the slurry, resulting in the improved flowability of the slurry.

- (3) AEA can reduce the viscosity and yield stress of the slurry. With the addition of AEA, both the viscosity and yield stress of the slurry decreased. In other words, AEA can improve the flow characteristics of fresh slurry. These results also prove the results of the slump and expansion tests.
- (4) AEA reduces the strength of the paste backfill sample, but it does not reduce it much. When the B content was 1.2%, the strength of the samples after 28 days of maintenance was reduced by 25.6%. According to the analysis of the strength test results, the number and volume of bubbles increase as the AEA content increases, which means that the voids inside the samples increase and cause the strength of the samples to decrease.
- (5) Considering the above experimental results and analysis, the strength requirement of the paste for the Linxi mine is 3 MPa. The final dosage of 0.9% B is the best choice, as it can change the flowability of the paste better and reduce the pipeline transportation resistance and transportation energy consumption. At the same time, the reduction in strength is also acceptable.
- (6) Further research is encouraged in the following areas:
  - (a) The mechanism of AEA affecting the flow properties and strength characteristics of paste made with gangue, fly ash, and cement should be studied using micro-experimental techniques.
  - (b) The effects of physical and chemical properties of gangue on the bubble shape and size distribution should be determined.
  - (c) Applicability of laboratory-scale results to field conditions should be considered.

**Author Contributions:** Conceptualization, X.W.; data curation, P.Y. and F.Y.; funding acquisition, B.Y., C.G., and T.L.; investigation, X.W., P.Y., and C.G.; methodology, B.Y. and C.G.; project administration, X.W. and X.Y.; resources, B.Y., X.Y., and F.Y.; supervision, F.Y.; validation, P.Y.; visualization, X.Y.; writing—original draft, X.W.; writing—review and editing, B.Y., X.W., and T.L. All authors have read and agreed to the published version of the manuscript.

**Funding:** This research received no external funding.

**Data Availability Statement:** Not applicable.

**Conflicts of Interest:** The authors declare no conflict of interest.

## References

1. Chen, J.; Zeng, B.; Liu, L.; Tao, K.; Zhao, H.; Zhang, C.; Zhang, J.; Li, D. Investigating the anchorage performance of full-grouted anchor bolts with a modified numerical simulation method. *Eng. Fail. Anal.* **2022**, *141*, 106640. [[CrossRef](#)]
2. Li, B.; Zhang, J.; Yan, H.; Zhou, N.; Li, M. Experimental investigation into the thermal conductivity of gangue-cemented paste backfill in mine application. *J. Mater. Res. Technol.* **2022**, *16*, 1792–1802. [[CrossRef](#)]
3. Qi, T.; Gao, X.; Feng, G.; Bai, J.; Wang, Z.; Chen, Q.; Wang, H.; Du, X. Effect of biomass power plant ash on fresh properties of cemented coal gangue backfill. *Constr. Build. Mater.* **2022**, *340*, 127853. [[CrossRef](#)]
4. Goswami, S. Impact of Coal Mining on Environment. *Eur. Res.* **2015**, *92*, 185–196.
5. Chen, J.; Liu, P.; Liu, L.; Zetng, B.; Zhao, H.; Zhang, C.; Zhang, J.; Li, D. Anchorage performance of a modified cable anchor subjected to different joint opening conditions. *Constr. Build. Mater.* **2022**, *336*, 127558. [[CrossRef](#)]
6. Zhang, X.; Feng, X.; Wang, Z.; Jian, J.; Chen, S.; Luo, W.; Zhang, C. Experimental study on the physico-mechanical properties and microstructure of foam concrete mixed with coal gangue. *Constr. Build. Mater.* **2022**, *359*, 129428. [[CrossRef](#)]
7. Zhu, X.; Gong, W.; Li, W.; Bai, X.; Zhang, C. Reclamation of waste coal gangue activated by *Stenotrophomonas maltophilia* for mine soil improvement: Solubilizing behavior of bacteria on nutrient elements. *J. Environ. Manag.* **2022**, *320*, 115865. [[CrossRef](#)]
8. Du, S.; Mao, S.; Guo, F.; Dong, K.; Shu, R.; Bai, J.; Xu, L.; Li, D. Investigation of the catalytic performance of coal gangue char on biomass pyrolysis in a thermogravimetric analyzer and a fixed bed reactor. *Fuel* **2022**, *328*, 125216. [[CrossRef](#)]
9. Liu, H.; Bai, G.; Gu, Y.; Yan, F. The influence of coal gangue coarse aggregate on the mechanical properties of concrete columns. *Case Stud. Constr. Mater.* **2022**, *17*, e01315. [[CrossRef](#)]

10. Zhu, M.; Qiu, J.; Chen, J. Effect and Mechanism of Coal Gangue Concrete Modification by Basalt Fiber. *Constr. Build. Mater.* **2022**, *328*, 126601.
11. Li, C.; Wang, S.; Zhang, X.; Wu, J.; Zheng, S.; Sun, Z. In-situ preparation of coal gangue-based catalytic material for efficient peroxymonosulfate activation and phenol degradation. *J. Clean. Prod.* **2022**, *374*, 133926. [[CrossRef](#)]
12. Li, G.; Deng, G.-Z.; Ma, J. Numerical modelling of the response of cemented paste backfill under the blasting of an adjacent ore stope. *Constr. Build. Mater.* **2022**, *343*, 128051. [[CrossRef](#)]
13. Wang, M.; Liu, L.; Wang, S.; Lv, B.; Zhang, B.; Zhang, X.; Zhao, Y.; Huan, C. Numerical investigation of heat transfer and phase change characteristics of cold load and storage functional CPB in deep mine. *Front. Earth Sci.* **2020**, *8*, 31. [[CrossRef](#)]
14. Qi, C.; Fourie, A. Cemented paste backfill for mineral tailings management: Review and future perspectives. *Miner. Eng.* **2019**, *144*, 106025. [[CrossRef](#)]
15. Saedi, A.; Jamshidi-Zanjani, A.; Darban, A.K.; Mohseni, M.; Nejati, H. Utilization of lead–zinc mine tailings as cement substitutes in concrete construction: Effect of sulfide content. *J. Build. Eng.* **2022**, *57*, 104865. [[CrossRef](#)]
16. Ghazi, A.B.; Jamshidi-Zanjani, A.; Nejati, H. Clinkerisation of copper tailings to replace Portland cement in concrete construction. *J. Build. Eng.* **2022**, *51*, 104275. [[CrossRef](#)]
17. Barzegar Ghazi, A.; Jamshidi-Zanjani, A.; Nejati, H. Utilization of copper mine tailings as a partial substitute for cement in concrete construction. *Constr. Build. Mater.* **2022**, *317*, 125921. [[CrossRef](#)]
18. Saedi, A.; Jamshidi-Zanjani, A.; Darban, A.K. A review of additives used in the cemented paste tailings: Environmental aspects and application. *J. Environ. Manag.* **2021**, *289*, 112501. [[CrossRef](#)]
19. Saedi, A.; Jamshidi-Zanjani, A.; Darban, A.K. A review on different methods of activating tailings to improve their cementitious property as cemented paste and reusability. *J. Environ. Manag.* **2020**, *270*, 110881. [[CrossRef](#)]
20. Tuylu, S. Effect of different particle size distribution of zeolite on the strength of cemented paste backfill. *Int. J. Environ. Sci. Technol.* **2022**, *19*, 131–140. [[CrossRef](#)]
21. Tuylu, S. Investigation of the Effect of Using Different Fly Ash on the Mechanical Properties in Cemented Paste Backfill. *J. Wuhan Univ. Technol.-Mater. Sci. Ed.* **2022**, *37*, 620–627. [[CrossRef](#)]
22. Li, T.; Wang, X.; Li, M.; Nan, D.; Shan, Q.; Chen, W. Synergy between suspending agent and air entraining agent in cement slurry. *Rev. Romana Mater.* **2020**, *50*, 344–353.
23. Yang, B.; Yang, J.; Yu, Y.; Li, D.; Jiang, B.; Cheng, K. Study on proportioning test of a new cementing filling material and hydration mechanism. *J. Min. Sci. Technol.* **2017**, *2*, 475–481. (In Chinese)
24. Wang, X.-M.; Zhao, B.; Zhang, C.-S.; Zhang, Q.-L. Paste-like self-flowing transportation backfilling technology based on coal gangue. *Min. Sci. Technol.* **2009**, *19*, 137–143. [[CrossRef](#)]
25. Kasap, T.; Yilmaz, E.; Sari, M. Effects of mineral additives and age on microstructure evolution and durability properties of sand-reinforced cementitious mine backfills. *Constr. Build. Mater.* **2022**, *352*, 129079. [[CrossRef](#)]
26. Wang, J.; Zhang, Q.; Yin, W.; Qi, S.; Gao, D.; Ma, D. On-Site Measurement on Compaction Characteristics of Coal Gangue and Surface Subsidence Disaster in Deep Backfilling Mining. *Front. Earth Sci.* **2021**, *9*, 724476. [[CrossRef](#)]
27. Wang, C.; Liu, Y.; Hu, H.; Li, Y.; Lu, Y. Study on filling material ratio and filling effect: Taking coarse fly ash and coal gangue as the main filling component. *Adv. Civ. Eng.* **2019**, *2019*, 2898019. [[CrossRef](#)]
28. Yin, W.; Zhang, K.; Ouyang, S.; Bai, X.; Sun, W.; Zhao, J. Experimental study on gangue backfilling materials improved by soda residue and field measurement of surface subsidence. *Front. Earth Sci.* **2021**, *9*, 1046. [[CrossRef](#)]
29. Feng, G.; Wang, Z.; Qi, T.; Du, X.; Guo, J.; Wang, H.; Shi, X.; Wen, X. Effect of velocity on flow properties and electrical resistivity of cemented coal gangue-fly ash backfill (CGFB) slurry in the pipeline. *Powder Technol.* **2022**, *396*, 191–209. [[CrossRef](#)]
30. Liu, L.; Fang, Z.; Qi, C.; Zhang, B.; Guo, L.; Song, K.I.-I.L. Numerical study on the pipe flow characteristics of the cemented paste backfill slurry considering hydration effects. *Powder Technol.* **2019**, *343*, 454–464. [[CrossRef](#)]
31. Yang, B.; Cui, X.; Sun, H.; Kong, L.; Kong, X. Study on the feasibility of coal mine void area cementation filling to control mining damage. *J. China Coal Soc.* **2000**, *343*, 361–365. (In Chinese)
32. Jin, J.; Qin, Z.; Lü, X.; Liu, T.; Zhang, G.; Shi, J.; Zuo, S.; Li, D. Rheology control of self-consolidating cement-tailings grout for the feasible use in coal gangue-filled backfill. *Constr. Build. Mater.* **2022**, *316*, 125836. [[CrossRef](#)]
33. Jiang, H.; Fall, M.; Yilmaz, E.; Li, Y.; Yang, L. Effect of mineral admixtures on flow properties of fresh cemented paste backfill: Assessment of time dependency and thixotropy. *Powder Technol.* **2020**, *372*, 258–266. [[CrossRef](#)]
34. Qiu, H.; Zhang, F.; Sun, W.; Liu, L.; Zhao, Y.; Huan, C. Experimental study on strength and permeability characteristics of cemented rock-tailings backfill. *Front. Earth Sci.* **2022**, *10*, 49. [[CrossRef](#)]
35. Hefni, M.; Hassani, F. Effect of air entrainment on cemented mine backfill properties: Analysis based on response surface methodology. *Minerals* **2021**, *11*, 81. [[CrossRef](#)]
36. Hefni, M.; Hassani, F. Experimental development of a novel mine backfill material: Foam mine fill. *Minerals* **2020**, *10*, 564. [[CrossRef](#)]
37. Puthipad, N.; Ouchi, M.; Attachaiyawuth, A. Effects of fly ash, mixing procedure and type of air-entraining agent on coalescence of entrained air bubbles in mortar of self-compacting concrete at fresh state. *Constr. Build. Mater.* **2018**, *180*, 437–444. [[CrossRef](#)]
38. Ke, G.; Zhang, J.; Tian, B.; Wang, J. Characteristic analysis of concrete air entraining agents in different media. *Cem. Concr. Res.* **2020**, *135*, 106142. [[CrossRef](#)]

39. Cao, L.; Shi, F.; Qiu, M.; Chen, W.; Cao, P.; Zhou, C. Effects of air entraining agent on the rheological properties and electrochemical parameters of cement mortar. *Constr. Build. Mater.* **2022**, *344*, 128233. [[CrossRef](#)]
40. Zhang, Y.; Gan, D.; Xue, Z.; Chen, X.; Hu, S. Effect of the initial air content in fresh slurry on the compressive strength of hardened cemented paste backfill. *Adv. Mater. Sci. Eng.* **2020**, *2020*, 8838572. [[CrossRef](#)]
41. Hassani, F.; Hefni, M.; Kermani, M.; Vatne, D. *Methods and Systems for Foam Mine Fill*; McGill University: Montreal, QC, Canada, 2016.
42. Hefni, M.; Hassani, F.P.; Kermani, M.F. A Review of the Properties of Foam Mine Fill. In Proceedings of the 13th ISRM International Congress of Rock Mechanics, Montreal, QC, Canada, 10–13 May 2015.
43. Jones, M.N. The interaction of sodium dodecyl sulfate with polyethylene oxide. *J. Colloid Interface Sci.* **1967**, *23*, 36–42. [[CrossRef](#)]
44. Yu, B.; Sun, J. Current synthesis of triterpene saponins. *Chem.-Asian J.* **2009**, *4*, 642–654. [[CrossRef](#)] [[PubMed](#)]
45. Koczurkiewicz, P.; Czyż, J.; Podolak, I.; Wojcik-Pszczola, K.; Galanty, A.; Janeczko, Z.; Michalik, M. Multidirectional effects of triterpene saponins on cancer cells—mini-review of in vitro studies. *Acta Biochim. Pol.* **2015**, *62*, 383–393. [[CrossRef](#)]
46. Yang, B.; Yang, H. Experimental study on the energy evolution characteristics of high-concentration cemented backfill in coal mine. *J. Min. Sci. Technol.* **2022**, *7*, 304–312. (In Chinese)
47. Zachl, A.; Buchmayr, M.; Gruber, J.; Anca-Couce, A.; Scharler, R.; Hochenauer, C. Air preheating and exhaust gas recirculation as keys to achieving an enhanced fuel water content range in stratified downdraft gasification. *Fuel* **2022**, *323*, 124429. [[CrossRef](#)]
48. Ouyang, X.; Guo, Y.; Qiu, X. The feasibility of synthetic surfactant as an air entraining agent for the cement matrix. *Constr. Build. Mater.* **2008**, *22*, 1774–1779. [[CrossRef](#)]
49. Zhang, L. Analysis on Slump and Expansion of Fresh Concrete by Cone Method and Spherical Defect Model. *Fly Ash Compr. Util.* **2018**, *5*, 140–142. (In Chinese)
50. Zheng, J.; Zhu, Y.; Zhao, Z. Utilization of limestone powder and water-reducing admixture in cemented paste backfill of coarse copper mine tailings. *Constr. Build. Mater.* **2016**, *124*, 31–36. [[CrossRef](#)]
51. Schackow, A.; Efftig, C.; Folgueras, M.V.; Güths, S.; Mendes, G.A. Mechanical and thermal properties of lightweight concretes with vermiculite and EPS using air-entraining agent. *Constr. Build. Mater.* **2014**, *57*, 190–197. [[CrossRef](#)]
52. Vatin, N.I.; Barabanshchikov, Y.; Komarinskiy, M.V.; Smirnov, S. Modification of the cast concrete mixture by air-entraining agents. *Inz.-Stroitel. Zhurnal* **2015**, *56*, 3–10. [[CrossRef](#)]
53. Du, L.; Folliard, K.J. Mechanisms of air entrainment in concrete. *Cem. Concr. Res.* **2005**, *35*, 1463–1471. [[CrossRef](#)]
54. Chen, J.; Qiao, M.; Gao, N.; Ran, Q.; Wu, J.; Shan, G.; Qi, S.; Wu, S. Cationic oligomeric surfactants as novel air entraining agents for concrete. *Colloids Surf. A Physicochem. Eng. Asp.* **2018**, *538*, 686–693. [[CrossRef](#)]
55. Yin, S.; Shao, Y.; Wu, A.; Wang, Z.; Yang, L. Assessment of expansion and strength properties of sulfidic cemented paste backfill cored from deep underground stopes. *Constr. Build. Mater.* **2020**, *230*, 116983. [[CrossRef](#)]
56. Zhang, D. Air entrainment in fresh concrete with PFA. *Cem. Concr. Compos.* **1996**, *18*, 409–416. [[CrossRef](#)]
57. Tunstall, L.E.; Ley, M.T.; Scherer, G.W. Air entraining admixtures: Mechanisms, evaluations, and interactions. *Cem. Concr. Res.* **2021**, *150*, 106557. [[CrossRef](#)]
58. Zhang, P.; Li, D.; Qiao, Y.; Zhang, S.; Sun, C.; Zhao, T. Effect of air entrainment on the mechanical properties, chloride migration, and microstructure of ordinary concrete and fly ash concrete. *J. Mater. Civ. Eng.* **2018**, *30*, 04018265. [[CrossRef](#)]
59. Belem, T.; Benzaazoua, M. Design and application of underground mine paste backfill technology. *Geotech. Geol. Eng.* **2008**, *26*, 147–174. [[CrossRef](#)]
60. Zhao, Y.; Taheri, A.; Karakus, M.; Chen, Z.; Deng, A. Effects of water content, water type and temperature on the rheological behaviour of slag-cement and fly ash-cement paste backfill. *Int. J. Min. Sci. Technol.* **2020**, *30*, 271–278. [[CrossRef](#)]
61. Koohestani, B.; Belem, T.; Koubaa, A.; Bussièrè, B. Experimental investigation into the compressive strength development of cemented paste backfill containing Nano-silica. *Cem. Concr. Compos.* **2016**, *72*, 180–189. [[CrossRef](#)]
62. Nasir, O.; Fall, M. Coupling binder hydration, temperature and compressive strength development of underground cemented paste backfill at early ages. *Tunn. Undergr. Space Technol.* **2010**, *25*, 9–20. [[CrossRef](#)]
63. Shah, H.A.; Yuan, Q.; Zuo, S. Air entrainment in fresh concrete and its effects on hardened concrete—A review. *Constr. Build. Mater.* **2021**, *274*, 121835. [[CrossRef](#)]
64. Gagné, R. Air Entraining Agents. In *Science and Technology of Concrete Admixtures*; Elsevier: Amsterdam, The Netherlands, 2016; pp. 379–391.
65. Holan, J.; Novák, J.; Müller, P.; Štefan, R. Experimental investigation of the compressive strength of normal-strength air-entrained concrete at high temperatures. *Constr. Build. Mater.* **2020**, *248*, 118662. [[CrossRef](#)]
66. Choi, P.; Yeon, J.H.; Yun, K.-K. Air-void structure, strength, and permeability of wet-mix shotcrete before and after shotcreting operation: The influences of silica fume and air-entraining agent. *Cem. Concr. Compos.* **2016**, *70*, 69–77. [[CrossRef](#)]
67. González, D.C.; Mena, A.; Mínguez, J.; Vicente, M.A. Influence of air-entraining agent and freeze-thaw action on pore structure in high-strength concrete by using CT-Scan technology. *Cold Reg. Sci. Technol.* **2021**, *192*, 103397. [[CrossRef](#)]
68. Qin, Y.; Hu, J.; Yang, D.; Kuang, Y.; Zhao, F.; Zhou, T. Optimization of transport performance and strength of the filling slurry in tailings reservoir waste by adding air entraining agent. *Minerals* **2020**, *10*, 730. [[CrossRef](#)]